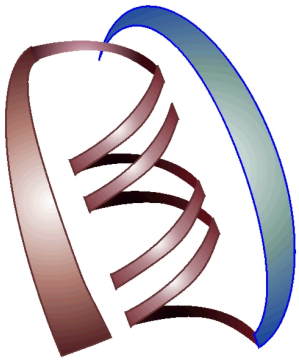

BIOMEDICAL
ENGINEERING

Carnegie Mellon University

2018 Biomedical Engineering Summer Undergraduate Research Symposium

August 1, 2018

Scott Hall 4N200

8:30 AM to 2:00 PM

Biomedical Engineering at Carnegie Mellon University
Biomedical engineering education at Carnegie Mellon reflects the belief that a top biomedical engineer must be deeply trained in both a traditional engineering practice and biomedical sciences. The unique additional major program leverages extensive collaborations with sister departments in the College of Engineering and with major medical institutions in Pittsburgh. This collaborative approach, combined with a rigorous engineering education, confers unique depth and breadth to the education of Biomedical Engineering graduates.

Biomedical Engineering Summer Undergraduate Research Program (BME SURP)
This program allows students to spend a ten-week period on a project that combines translational research and clinical exposure at a local medical center. Hundreds of students have participated in BME-SURP since its introduction in 1980. The experience have played a major role in helping students choose their career paths and obtain positions in industrial or academia. This program is supported by grants from the CMU College of Engineering This program is supported by grants from the CMU College of Engineering and the CMU University Research Office (URO).

Carnegie Heart Program
The Carnegie Heart Program is a collaborative effort between the Biomedical Engineering Department at Carnegie Mellon University and the Allegheny Health Network. The purpose of this program is to develop biomedical engineers who can apply their education toward new technologies for clinical cardiovascular medicine. In addition to students' experience in a laboratory setting, students will shadow cardiovascular clinicians at Allegheny General Hospital one day approximately every two weeks. This program is supported through a grant from the American Heart Association.

Presentation Schedule

8:30 AM to 9:00 AM Breakfast

9:00 AM: Mia Keyser (BME-SURP/URO)

9:15 AM: Paul Kim (BME-SURP/URO)

9:30 AM: Kara Nickolich (BME-SURP/URO)

9:45 AM: Dominique Petach (BME-SURP/URO)

10:00 AM: Pirapat Rerkpattanapipat (BME-SURP/URO)

10:15 AM to 10:30 AM: Break

10:30 AM: Annie Yang (BME-SURP/URO)

10:45 AM: Olivia Olshevski (Carnegie Heart)

11:00 AM: Erin Kavanagh (Carnegie Heart)

11:15 AM: Alisha Lokhande (Carnegie Heart)

11:30 AM: Michael Hall (Carnegie Heart)

11:45 AM: Cameron Pitts (Carnegie Heart)

12:00 PM to 12:45 PM: Lunch

12:45 PM: Liliana Santizo Deleon (BME-SURP)

1:00 PM: Shanley Lenart (BME-SURP)

1:15 PM: Shinjini Ray & Gabriela Perez-Lozano (BME-SURP)

1:30 PM: Courtney Ollis (BME-SURP)

1:45 PM: Andrew Febrillet (BME-SURE)

2:00 PM Cake!

Xuanyu Min (BME-SURP/URO) presented earlier at a separate presentation

Title: Investigation of Artificial Food Dyes as Potential Obesogenic Chemicals
Authors: Mia Keyser, Megan DeBari, Rosalyn Abbott

Introduction: A significant health issue plaguing modern society is the prevalence of obesity; according to 'The State of Obesity Project,' approximately 38% of American adults are obese and approximately 31.2% of American children are overweight or obese. Despite current initiatives to encourage the public to lead healthier lives, obesity remains more than just a personal health and wellness issue, as environmental factors, such as what we consume in modern society, have a significant effect on human physiology. There are many chemicals used in the American food production industry that are regularly put on or into foods that have not been tested for physiological effects. Such chemicals could be a subset of endocrine disrupting chemicals called obesogens, which negatively alter lipid-related metabolic activities and cause humans to have a predisposition to developing obesity. A group of chemicals in the food production industry that have not been screened for their physiological effects concerning adipose tissue are artificial food dyes. The use of artificial food dyes have increased significantly since the 1950s and they have been proven to have effects on human physiology and behavior, especially in children [2]. Thus, it is pertinent to investigate these chemicals in relation to their metabolic effects and obesity, as the consumption of artificial food dyes and the obesity epidemic have both been increasing with time. This study aims to determine if artificial food dyes are obesogens.

Materials and Methods: Silk fibroin (cocoons sourced from the UK) was formed into silk sponges via the water-based methodology as described previously [1]. Scaffolds were cut (2mm x 4 mm) and seeded with either complete adipose tissue, adipocytes, or adipose derived stem cells (hASCs), all sourced from a human panniculectomy. Microenvironments were cultured for 10 days in minimally supplemented media (Phenol red free DMEM/F12, 10% Charcoal-Stripped FBS, 1XPSF) containing varying concentrations of artificial food dye exposure (0.1uM, 1uM, 10uM, and 100uM exposure for each artificial food dye tested). Unsupplemented media was used as a negative control while 10 µM BPA, and 1 nM TBT media were used as positive controls. To quantify cell growth, intracellular lipid accumulation, and lipolysis, DNA content, triglyceride content, and glycerol secretion were quantified with PicoGreen (Invitrogen), Triglyceride (BioAssay Systems), and Adipolysis Assays (BioAssay Systems), respectively. A Zeiss LSM 700 Confocal was also used to image microenvironments for qualitative analysis of cell growth. Such characteristics along with statistical evaluation of data served as the basis of determining obesogenic effects.

Results and Discussion: Preliminary results of DNA content of scaffolds indicate that all scaffolds were successful in sustaining cell cultures (Figure 1). Additionally, the DNA content of the scaffolds suggest that the number of cells contained in the control scaffolds for the adipocytes and hASCs cell culture groups were not statistically different then the number of cells contained in the artificial food dye exposed scaffolds. However, for complete adipose tissue microenvironments, the results indicate the artificial food dye exposed scaffolds contain more cells in comparison to control groups. This suggests that the artificial food dye may have some influence on the proliferation of one or more cell types in the composition of complete adipose tissue.

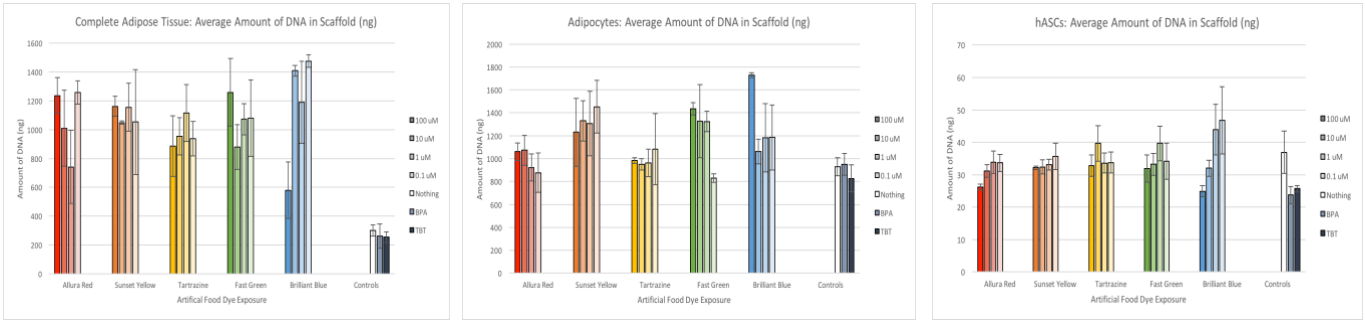

Figure 1. Average amount of DNA in scaffolds, grouped by cell culture type, artificial food dye, and media exposure concentration.

Conclusion: Though an effect on cell proliferation in complete adipose tissue was observed in response exposure to artificial food dyes, future assays examining glycerol secretion and triglyceride content, along with imaging and statistical analysis, will determine whether there was an altered metabolic response to the exposure.

Acknowledgements: The authors would like to thank Sean Pereira and Olivia Olshevski for technical assistance.

References:
[1] Rockwood D N, *Nature America*, 2011, 6, 1612-30
[2] Simmons A L, *Curr Obes Rep*, 2014, 3, 273-85

Effect of Orbital Shaking on Rheological Behavior of Regenerated Silk Fibroin Solutions

Paul K. Kim[1], Rosalyn D. Abbott[1], Megan K. DeBari[1]
[1]Carnegie Mellon University, Pittsburgh, PA

Introduction: Hydrogels made from natural sources are highly desirable for a variety of tissue regeneration and drug delivery applications. Natural, biopolymeric hydrogels have greater biocompatibility than those prepared from synthetic materials, while having equally high mechanical strength. The two key factors for these hydrogels are tunability of mechanical properties and ability to precisely control the gelation kinetics, which allow for uniform encapsulation of cells *in vivo* with high spatial precision. Regenerated silk fibroin (RSF) solution has been used to prepare hydrogels with tunable mechanical properties and degradation rates that can be adjusted under varying treatment conditions. However, RSF is highly sensitive to those conditions; past studies noted that even weak shear stress, such as shaking, applied on RSF solution may have profound effect on its gelation, which may yield hydrogels with less predictable properties. The effects of shaking, however, have not been examined in detail. To confirm suggestions from previous studies, this study assessed the effect of shaking on mechanical properties of RSF solutions, by analyzing their rheological behaviors in response to varying duration of shaking.

Materials and Methods: First, *Bombyx mori* cocoons were degummed in boiling Na_2CO_3 solution (0.02 M) for 30 minutes, rinsed with deionized water and dried overnight to remove sericin from silk fibers. The fibers were then dissolved in LiBr solution (9.3M) and purified via dialysis against deionized water for 3 days. The resulting silk fibroin aqueous solution was ~8.71% (w/v). The solution was subjected to shaking at 150 rpm for 90, 120, 150, 180, and 210 minutes, using an orbital shaker (Model 361, Fisher Scientific), in 4 °C to minimize temperature effects. Immediately after shaking, samples for each shaking time were placed into a syringe for loading onto rheometer plate and were stored in 4 °C at all times throughout the experiment. The viscoelastic properties of each sample were evaluated using a DHR rheometer (TA Instruments) at 25 °C. To observe any possible time dependency of shaking on the samples, same rheological tests performed the next day.

Results and Discussion: Silk fibroin is an amphiphilic polymer that self-assembles into micelles in solution. Shaking accelerates the self-assembly by allowing for more interactions among fibroin molecules in solution, hence more physical crosslinks. Rheological test results confirmed this theory; immediately upon shaking, the solution became more fluidic, perhaps due to transient dispersion of fibroin in solution (Figure 1(a)). After some time (>120 min), the stiffness of the solution was partially recovered. The dynamic moduli of the shaken solution evidently increased following overnight storage at 4°C, beyond those of the control, though only by less than one order of magnitude (Figure 1(b)). Such behavior can be attributed to increased β-sheet content resulting from more interaction among fibroin molecules. The flow sweep data correlated well with the oscillatory data, as the estimated zero-shear viscosity increased with shaking time after overnight storage (Figure 1(c)). Under higher shear rates, however, the solutions reached a consistent value of viscosity, regardless of shaking time.

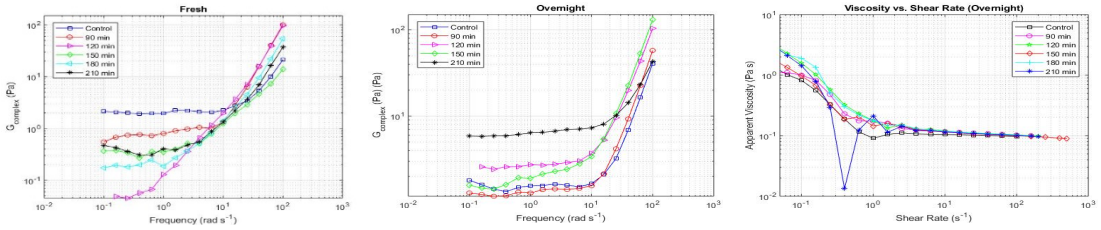

Figure 1: (a) Immediately after shaking, complex modulus $|G^*|$ of RSF solution decreased as shaking time increases. (b) $|G^*|$ effectively increased after overnight storage, beyond that of the control. (c) Apparent viscosity of RSF solution as function of shear rate. No large deviations from the control were observed.

Conclusions: Though evidently higher stiffness in RSF solution was obtained by shaking and overnight storage, the change in bulk behavior of the solution was minor, almost negligible under large deformation. In future work, the effect of storage time on shaken solutions will be further investigated until gelation is observed. Further bulk rheological tests and microstructural studies will be done on the resulting hydrogels to investigate any structural changes in the molecular level. In addition, since natural gelation of RSF can take months, the potential application of orbital shaking in reducing gelation time for RSF hydrogels will be studied.

Detection of *Aspergillus fumigatus* RNA by quantitative reverse transcription PCR

Kara Nickolich

Introduction: While *Aspergillus fumigatus* is thought to predominantly infect immunocompromised patients, recent clinical reports have documented an increase in influenza-*A. fumigatus* superinfection related hospitalizations and deaths in immunocompetent patients. A mouse model for this type of superinfection is being developed, and current quantification of fungal burden is done by counting colony forming units (CFUs) from lung homogenates. This quantification can under-represent the amount of *A. fumigatus* present, as the homogenizing process used the break apart the animal tissue can shear the fungal hyphae and decrease fungal vitality. Previous studies have used quantitative reverse transcription PCR (RT-qPCR) of the *A. fumigatus* 18s rRNA gene as a more accurate method of quantifying *A. fumigatus* burden. To determine the viability of using RT-qPCR to measure Aspergillus fumigatus in a influenza-fungal superinfected mice, I am optimizing a protocol for extracting RNA from *A. fumigatus* cells and subsequent RT-qPCR analysis.

Materials and Methods: *A. fumigatus* was grown for five days on potato dextrose agar (PDA) before being re-suspended in phosphate-buffered saline (PBS). Cells were lysed with one of three methods: flash frozen in liquid nitrogen and crushed with a mortar and pestle, homogenized with a rotary homogenizer, or lysed with bead beating. The three RNA isolation kits used were MasterPure, Qiagen, and Agilent and both the quantity and quality of extracted RNA was assessed. Isolated RNA concentrations were measured on a NanoDrop and cDNA was made using a Bio-rad iScript kit. The 18s gene was measured with RT-qPCR on a Bio-rad PCR thermocycler using primers as previously described by Zhao et al.. RNA and cDNA were run on 0.8% agarose gels and illuminated with ethidium bromide to confirm RNA quality and DNA amplification of a unique PCR product.

Results and Discussion: Results showed that bead beating was the best method of fungal RNA isolation, with respect to both quantity and quality. Of the three RNA isolation kits tested, the MasterPure and Qiagen kits were able to extract the RNA from *A. fumigatus*, with the Qiagen kit containing less genomic DNA contamination. Preliminary test runs of the 18s gene using RT-qPCR showed that the probe was giving a weak signal in a pattern that suggested inconsistent binding to the cDNA. This was corrected by increasing the probe concentration and the extension time. RT-qPCR with the 18s gene was repeated and showed consistent binding of the primer and probe across technical replicates.

Conclusions: By determining a reliable method of fungal RNA isolation and a functional utilization of the 18s gene present in *A. fumigatus*, we can now begin to examine the possibility of isolating fungal RNA from within the lung tissue of the mouse model and obtain an accurate quantification of fungal burden, which is necessary for the study of Influenza-fungal superinfection. We will then use the mouse model of influenza-*A. fumigatus* co-infections to investigate the hypothesis that preceding influenza infection attenuates the expression of cytokines and recruitment of immune cells necessary to clear *A. fumigatus.*

References:

- Griffiths L, Anyim M, Doffman S, Wilks M, Millar M, Agrawal S. J. Med. Microbiol. 55(9):1187-1191
- Shah M.M., Invasive pulmonary aspergillosis and influenza co-infection in immunocompetent hosts: case reports and review of the literature, Diagnostic Microbiology and Infectious Disease, Volume 91, Issue 2, 2018, Pages 147-152.
- Sheppard D.C., Comparison of three methodologies for the determination of pulmonary fungal burden in experimental murine aspergillosis, Clinical Microbiology and Infecttheresporeion, Volume 12, Issue 4, 2006, Pages 376-380.
- Zhao Y., Detection of Aspergillus fumigatus in A Rat Model of Invasive Pulmonary 2 Aspergillosis by Real-time Nucleic Acid Sequence-Based Amplification (NASBA) 3 4.

Introduction: In the world today, almost 115,000 people are in need of a lifesaving organ ("Technology for Transplantation", 2018). Unfortunately, the patient to donor ratio is heavily skewed, resulting in a high demand for donor organs. As a result, bioengineering organs is becoming extremely prevalent as it eliminates the need of a donor. Currently, vasculature functionality is greatly reduced in bioengineered organs as well as transplanted organs. This is due to a loss in vitality of the glycocalyx, an essential layer which lines the endothelial cells in blood vessels.

Materials and Methods: We have hypothesized that, using two different methods, the glycocalyx can be regenerated in cultured endothelial cells and prevented from becoming internalized in the cell as well. Two methods will be studied: using a DNA-heparin hybridization technique and another method with a heparin conjugate with no DNA. Both methods consist of layer-by-layer growth of the glycocalyx.

Results and Discussion: We successfully labeled the cell surface with azide, and then labeled the azide surface with a single stranded DNA. Also, we have labeled the cell surface with a heparin conjugate. We are still working on conjugating heparin to DNA.

Conclusions: Once the glycocalyx, and thereby the vasculature is restored in vitro, this technique can be applied to bioengineered organs and transplanted organs. This will hopefully restore the functionality of the vasculature and remove the worry for patients to find an organ when the times comes.

Acknowledgements: These studies were supported in part by the funding of Carnegie Mellon University's SURF grant.

Utilizing Fibroin Silk Solution To Improve Biocompatibility And Mechanical Properties Of Artificial Lungs

Max Rerkpattanapipat

Introduction: Over 120,000 lives are taken each year due to chronic lung diseases. The only long-term treatment for chronic lung diseases is lung transplantation. However, there is a shortage of donor organs. Dr. Keith Cook and his lab have developed artificial lung models that can potentially be implanted into patients with acute respiratory insufficiency or end-stage pulmonary diseases, which would provide them with sufficient oxygen and carbon dioxide transfer. These models have the potential to be successful, however, one of the main roadblocks is clotting due to limited biocompatibility. The goal of this project is to utilize silk as a drug eluting material that will secure fiber mats of the artificial lung model. Currently, weaving fibers that do not participate in gas exchange hold the hollow gas exchange fibers together. These weaving fibers are observed to be a clot propagation point - a huge problem for the devices. Through this study our team investigated a method of producing fiber mats that includes using silk to secure the hollow gas exchange fibers into the ideal position. Silk is highly biocompatible and shows very low blood activation as is, but to make the silk material even more useful in a blood-contact setting, we plan to load it with Factor XII inhibitor, a drug which will further prevent clotting to an artificial surface. With this solution, we have a stable and biocompatible material replacing our weaving fibers and drug delivery of an intrinsic coagulation cascade inhibitor.

Materials and Methods: The first phase was to produce fibroin silk solution through extraction of silk from silkworm cocoons. This required cutting up the cocoons and placing it in a near boiling sodium carbonate solution for half an hour. Once completed coccoons were broken down into cotton-like silk strands. The following step required packing the silk strands into a 100 mL beaker and pouring a layer of lithium bromide solution over the silk. This mixture was then placed into the oven for four hours. Upon completion of heating, the silk will have been broken down into the desired viscous fibroin silk solution. The final steps of fibroin silk solution synthesis consisted of desalinating the soluition via dialysis cassetes followed by centrifuging the solution. The experimental phase involved lining out 1 mL fibroin solution strands from the batches onto aluminum foil in varying temperature environments. The ultimate goal was to observe the optimal concentration of silk and temperature environment that most effectively solidified the solution into the desired glue material to secure the gas exchange fibers.

Results and Discussion: Solidification of fibroin silk solution silk strands was found to be most successful at high silk concentration and low temperature environment conditions. Batch B (12.5% concentrated) ultimately evaporated because it was relatively dilute, leaving insufficient amount of fibroin silk behind to combine into noticeable beta sheets regardless of temperature. Batch A (25% concentrated) solidified at all temperatures but to different extents. Solidification was most stable at lower temperatures and became more brittle with rising temperature. At cold temperatures the solidified silk strands even presented with some elasticity character. It appears that high silk concentration and low temperature set up ideal environment for fibroin silk to productively form strong beta sheets. Now that an effective method of silk solidification has been confirmed, testing the fibroin silk strand effectiveness in securing gas exchange fibers can proceed. This is being performed via *in vitro* blood incubation testing of fiber mats held together by the fibroin silk instead of the traditional weaving fibers.

Fibroin Silk Solution Solidification Outcomes in Varying Concentrations and Temperatures

	Fibroin Silk Solution Concentration	
Temperature	25% Concentrated (Batch A)	12.5% Concentrated (Batch B)
Low Temp (4 C)	Solidified - Relatively sturdy and elastic (n=5)	Evaporated (n=5)
Room Temp (23 C)	Solidified - Relatively sturdy, not very elastic (n=5)	Evaporated (n=5)
Body Temp (37C)	Solidified - Brittle (n=5)	Evaporated (n=5)

Table 1. Summarizes the qualitative outcomes of strands from 25% and 12.5% concentrated fibroin silk solution batches in different temperature environments. Batch A strands solidified to different extents at all temperatures while Batch B strands ultimately evaporated at all temperatures.

Conclusions: Fibroin silk solution can be effectively utilized as biological glue on the Cook Lab's artificial lung fiber mats upon solidifying through the combination of high fibroin silk concentration and low temperature. This discovery enables for proceeding in evaluating whether the fibroin silk glue will improve the biocompatibility of the artificial lung model.

References: **[1]** Yucel, T. *et al.* J. Control Release 2014, 190, 381-397. **[2]** Ming, J. *et al.* Int. J. of Biological Macromolecules 2015, 75, 398-401.

Acknowledgements: Many thanks to the Carnegie Mellon Undergraduate Research Office, the Carnegie Mellon Biomedical Engineering Department, Kalliope Bouloubassis, and Dr. Keith Cook for providing the funding, resources, and support to making this summer undergraduate fellowship research project possible.

Annie Yang
BME SURP-URO

Abstract
July 26, 2018

Introduction

As science and research advances with the dangers and risks of diseases and illnesses, targeted therapeutics and more selective methods of treatments are explored. Production of antibodies, selective proteins that play a major role in immune response, are of high demand in many applications of targeted therapy. Antibodies are produced by hybridoma cells, which are cells that are very sensitive to their environment. Different factors of the culture can dramatically affect the efficiency of antibody production. A decline in total number of hybridoma cells is observed after several days of culture. Different parameters, such as number of days of culture, different cell densities, and various forms of agitation, are analyzed to find the optimal conditions for mass production of antibodies. Success in antibody production can lead to reduction in inflammation and rejection in not only tissues but whole transplanted organs.

Materials and Methods

Mouse hybridoma cells that secrete anti-human tumor necrosis factor alpha (anti-TNF-a) antibodies were cultured in a media containing RPMI P/S + 5% FBS. To investigate if hybridoma cell culture densities and days of culture affect antibody production, different cell densities of 1.0×10^6, 2.0×10^6, and 5.0×10^6 cells/mL were plated. Cell count was performed daily to measure cell viability and the supernatant containing the antibody was collected for a period of 1, 2, 3, 6, and 9 days and analyzed. The amount of antibodies generated was semi-quantitated using Western blot analysis. The anti-TNF-a antibodies are detected using a chemiluminescence, and analyzed with ImageJ. Static hybridoma culture may lead to unequal distribution of nutrients and oxygen, which can contribute to lower cell viability over time. To investigate this hypothesis, two forms of gentle agitation was applied to the cell cultures to ensure homogenous cell distributions: an orbital shaker and a magnetic spinning rod. Ultimately, the collected antibodies were purified and analyzed with the SYPRO Ruby Protein Gel Staining kit.

Results and Discussion

Our Western blot results showed that at a high cell density of 5×10^6 cells/mL, there is a greater antibody production, in comparison to that at 2×10^6 and 1×10^6 cells/mL at day 3. Nonetheless, the viability of the hybridoma cells dramatically decreased after the third day, resulting in a significant reduction in antibody production regardless of initial cell density. As for Day 9 cultures, all the cells were no longer viable, and therefore, the supernatants were not analyzed. High cell density may not be suitable for long-term antibody production due to higher competition on nutrients and oxygen. To further elucidate the hypothesis that depletion of nutrients and oxygen occurs in high cell density cultures, we cultured the hybridoma cells treated on an orbital shaker with speed of 69 rpm. With agitation, there can be a more homogenous distribution of nutrients and oxygen, promoting proliferation and antibody production.

Conclusion

Optimal parameters are needed to mass produce antibodies that can be used in various fields, such as pharmaceuticals. Preliminary data highly suggests that the higher the density of hybridoma cells cultured, the greater the antibody production as of Day 3 and 6. However, even at densities as low as 1.0×10^6 cells/mL, cell viability decreases dramatically after Day 6 of culture. Further research on providing agitation to the cell cultures in hopes of increasing cell viability is currently underway.

Olivia Olshevski

Introduction: With heart disease as the leading cause of death in both men and women worldwide, it is essential to find an alternative approach to cardiac repair and replacement, as current methods require donor hearts that have insufficient supply or introduce non-native materials into the body. One way to do this is to fabricate an extracellular matrix (ECM) scaffold onto which cardiomyocytes (CMs) can be seeded to produce fully functional cardiac sheets. To provide immature CMs, obtained by differentiating human pluripotent stem cells, with ECM cues to properly align them, we need to build a biomimetic scaffold from the bottom-up. However, while soft lithography has been used to create complex ECM patterns with micrometer size features in 2D, 3D cardiac tissues have instead relied on homogenous bulk hydrogels which offer no control over structure at the cellular level and generate an insufficient and unreliable contractile force. Here we propose a method to engineer highly aligned 2D sheets of cardiomyocytes supported by native ECM materials that can be stacked to create 3D tissues.

Materials and Methods: To bridge the gap between 2D and 3D techniques, a novel technique to micropattern ECM cues onto collagen I hydrogels is used. To do this, surface-initiated assembly is utilized in order to release microcontact-printed ECM proteins from the substrate, thereby allowing the patterns to be transferred to the hydrogels. First, fibronectin (FN), an ECM component, is microcontact printed in a standard pattern of 20 um wide by 20 um spacing lines (20x20) onto a glass coverslip coated with poly(N-isopropylacrylamide) (PIPAAm). Because PIPAAm, a thermoreversible compound, dissolves in water at room temperature, it is then possible to transfer the ECM pattern to other substrates. Using this characteristic, FN lines originally printed onto the PIPAAM coverslips are then transferred to collagen I hydrogels in order to microfabricate the ECM scaffolds. In doing so, the complex 3D organization of ECM cues found *in vivo* can be reproduced layer-by-layer with precision similar to that seen in 2D approaches. CMs, obtained from differentiating the HES3 human embryonic stem cell line, can then be seeded onto these ECM scaffolds to create cardiac sheets with unique alignments. By stacking these sheets, a 3D structure can be obtained and analyzed for the contractile force produced as well as the degree of alignment between the actin cytoskeleton of the CMs and the patterned FN lines.

Results and Discussion: FN lines were successfully transferred to collagen I hydrogels. Cardiomyocytes were seeded onto collagen hydrogels with FN lines at a density of 300,000 cells/cm^2 and cultured for 4 days before fixing and staining the samples. After imaging the samples using a Zeiss LSM700 laser scanning confocal microscope using a 20X objective, little to no alignment of the CMs with the FN lines was qualitatively found, though cells had properly attached to the ECM scaffolds. Though more research must be performed to make any definitive claims, it is suspected that the highly passaged cells (P9 prior to seeding) and a small seeding density doubly contributed to this lack of alignment.

Conclusion: Additional samples must be analyzed before a final conclusion can be made as to whether or not FN nanofiber-based hydrogel scaffolds can be applied to the creation of laminar cardiac tissue. Future studies include stacking the cardiac sheets, analyzing their contractile force generation, and quantifying their alignment with the micropatterned FN lines in order to determine the similarity of our fabricated cardiac tissue constructs to native cardiac tissue. If successful, these cardiac sheet structures, composed of materials which make them directly implantable and uniquely aligned layer-by-layer to mimic ECM cues of the native embryonic myocardium, may serve as a viable alternative for cardiac replacement and repair.

Erin Kavanagh

Introduction: Hypertension affects approximately 1 in 4 people in the U.S. and left untreated alters the physical structure of cerebral blood vessels[1]. This change in the morphology of cerebral blood vessels disrupts cerebral autoregulation[2], the physiological mechanisms that maintain blood flow in the brain at an appropriate level during changes in cerebral perfusion pressure, which is the difference between mean arterial blood pressure and intracranial pressure. This leads to a much higher risk of stroke and is the single biggest risk factor for suffering from a stroke, causing about 50% of ischemic strokes.[3] In order to quantify cerebral autoregulation, one must measure intracranial pressure (ICP). We want to show that the hemodynamic response to cerebral perfusion pressure (CPP) changes can be used to calculate non-invasive ICP changes through non-parametric transfer function analysis. By measuring ICP, the hope is this can be used as an indicator of cerebral health and a predictor for better neurological outcomes in traumatic brain injury, stroke, and hydrocephalus cases.

Materials and Methods: Near-infrared spectroscopy (NIRS) is an optical technique which can measure the concentration of cerebral oxygenated (HbO_2) and deoxygenated (Hb) hemoglobin non-invasively. Light at 690 and 830 nm is directed through the skull and reflected light which has interacted with the brain is collected by a detector. Since the absorption spectra of HbO_2 and Hb are distinct from each other, the two hemoglobin species can be differentiated. A three-point sensitivity process is used to create a spatial sensitivity profile, with a modified version of the Beer Lambert Law (1) taking into account the high scattering in the extra path.

$$\Delta\mu_a(\lambda) = -\frac{1}{r\mathrm{DPF}}\frac{\Delta I(\lambda)}{I_0} \qquad (1)$$

In-vivo studies on sedated Rhesus Macaque were conducted and ICP, HbO_2, Hb, and ΔHbO_2 and ΔHb were measured over time. ICP changes were induced by 3-5 cc fluid injections. The data is run through MATLAB with a high pass filter from 1.7 to 2.4 Hz), and a curve fitting function *fittype('exp2')* with markers placed in the data set fit the ICP, ΔHbO_2 and ΔHb oscillations with linear and exponential curves to predict the recovery time of ICP**.**

Results and Discussion: The best overall fit for the ICP, ΔHbO_2 and ΔHb oscillations was found to be a second order exponential. This produced the highest R^2 value when compared to the linear fit and was able to show a systematic downwards trend in oscillation slopes. Figure 1 shows an example data set, where ICP recovered during systematic increases over time. It was observed that as baseline ICP increased, the slopes also increased, thus recovery time became faster. In conclusion the higher ICP became, the faster it recovered to baseline.

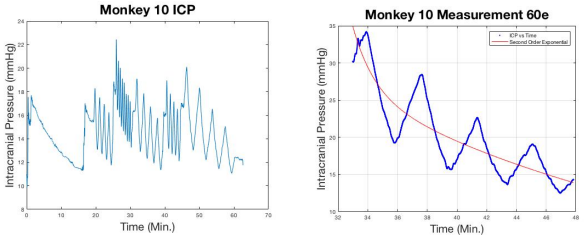

Figure 1. (left) Filtered intracranial pressure with oscillation (right) fitted with second order exponential

Conclusions: We demonstrated that MATLAB curve fittings can potentially predict ICP and hemodynamic changes. This was done using a hydrocephalus non-human primate model with strong oscillation magnitudes in ICP, causing subsequent reactions in HbO_2 and Hb as well. It can be concluded that the oscillations in ICP can be used to predict ICP drop-off rate. Thus, the oscillatory slopes found in ICP and other hemodynamic data could be used to generate future data points and thus be used by physicians to predict neurological outcomes.

Acknowledgements: I would like to thank PhD student Alexander Rüsch and Dr. Jana Kainerstorfer for their knowledge and support in this research project.

[1] Li, Yunxia. "Cerebral Angiography, Blood Flow and Vascular Reactivity in Progressive Hypertension." *NeuroImage* 111: 329–337.
[2] Girouard, Helene. "Neurovascular Coupling in the Normal Brain and in Hypertension, Stroke, and Alzheimer Disease." *JAP*, vol. 100, no. 1,pp. 328–335
[3] "High Blood Pressure and Stroke." *Stroke Association*, Sept. 2012, www. stroke.org/uk/sites/default/files/high blood pressure and stroke.pdf.

Prototyping a Soft Robotic Bi-ventricular Copulsation Sleeve through 3D Printing

Main Contributors: Alisha Lokhande, Jooli Han, Dr. Dennis Trumble

Introduction

As one of the leading causes of death in America, congestive heart failure (CHF) affects over 6.5 million adults within the US alone. With projections increasing year after year, CHF has developed into a public health problem with 50% of adults estimated to die within 5 years of diagnosis. While common treatments include heart transplants and ventricular assist devices (VADs), the selectivity with receiving a donor heart and long-term complications with current VADs demonstrates sufficient need for a new self-contained and non-blood-contacting VAD. One such device proposed by the Trumble Lab at Carnegie Mellon University is a soft-robotic bi-ventricular sleeve powered through muscle energy conversion. Through inflation of hollow chambers along the device perimeter, the application of hydraulic pressure to the ventricular epicardium has the potential to increase the ejection fraction of a failing heart. The goal of this project is to prototype a preliminary working model of the given theoretical design to demonstrate feasibility of fabrication using 3D printing technology.

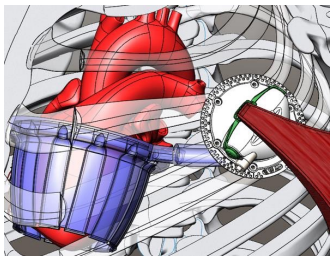

Figure 1. 2D Bi-ventricular Sleeve Model. Conceptual drawing of device with muscle energy converter attached inline with latissimus dorsi muscle.

Materials and Methods

For prototype fabrication, the main 3D printing techniques used were Stereolithography (SLA) and Fused Deposition Modeling (FDM). Printers were selected based on their support of flexible material with appropriate physical characteristics (low durometer). Prior to printing, simplified SolidWorks sleeve models were configured in printer-specific softwares to generate supports and export compatible files for the printers. The SLA 3D printers included an AutoDesk Ember (SM 472) and a FormLabs Form2 (Flexible Resin). The two FDM 3D printers were a LulzBot (NinjaFlex) and an Ultimaker3 (Semi-Flexible TPU and Polymaker PolyFlex). Post-processing was conducted for all parts including the removal of excess material and supports. As the original SolidWorks design was modified, this process was repeated for all printers to yield improvements with each iteration. Each material and printer was then qualitatively assigned a score from 0 to 3 based on the products as working prototypes. Such criteria included the presence of local defects, removability of supports, and potential for further improvements.

Results and Discussion

Among the 3D printers and flex materials used, the quality scores ranged from 1 to 2.5 out of 3. The lowest quality model was the Ember printer with build area restrictions causing the model to be significantly scaled down. The highest rated models were the Flexible Resin from the Form2 and the PolyFlex and Semi-Flexible from the Ultimaker3. The former had the highest general print quality with the lowest material durometer; however, internal supports could not be removed during post-processing. The Ultimaker models had a lower print quality as a result of the volume of material available; however the PVA supports were water-soluble and the main materials exchangeable. All models displayed localized defects. Main challenges arose in printing the hollow and enclosed structures, the removal of internal supports, and general difficulties associated with using flexible materials.

3D Printer	Material	Printer Type	Score
Form2	Flexible Resin	SLA	2.5
Ember	SM 472	SLA	1
Ultimaker3	PolyFlex	FDM	2.5
Ultimaker3	Semi-Flexible	FDM	2.5
LulzBot	NinjaFlex	FDM	2

Table 1. Quality Score by 3D Printer and Flexible Material.

Conclusion

From this project, the capability to fabricate preliminary designs of the bi-ventricular sleeve using 3D printing has demonstrated potential although major limitations from material selection and properties remain. The Ultimaker3 printer was found to have the highest potential to produce working prototypes as a result of the ability to exchange main filaments and dual extrusion accommodating soluble supports. In the future, further explorations with lower durometer, flexible materials that are Ultimaker-compatible are suggested to develop improved sleeve prototypes.

Acknowledgements

I would like to thank my graduate student advisor, Jooli Han, and Dr. Dennis Trumble for their invaluable guidance and support throughout the duration of this project. I would also like to thank the BME Department at CMU and the American Heart Association for their financial support toward the Carnegie Heart Fellowship.

Fuzzy Graphene Characterization for Photothermally Stimulating Cardiomyocytes

Michael Hall

Introduction: Cardiac electrophysiology is the study of elucidating, diagnosing, and treating electrical activity within the heart. Electrophysiology studies (EPS) are tests that allow doctors to understand abnormal heart rhythms known as arrhythmias. These tests help to analyze the location of an arrhythmia and what is necessary to treat it by creating an electrical stimulus in the heart and measuring its activity usually via an inserted specialized electrode catheter. Electrical stimulation is important for exploring and manipulating cardiac cell behavior through the generation of action potentials (APs) and is widely used for both research and therapeutics. Photothermal stimulation can be used rather than electrical stimulation to obtain higher spatial and temporal resolution, effectively reducing the chances of artifact. Current techniques of optically driven cell control involve photoactive mediators or the use of external photoactive materials placed in close proximity of cells.[1] The purpose of this study is to obtain improved photothermal response by introducing nanoscale textures to silicon nanowires (SiNWs) creating a material called fuzzy graphene (3DFG) considered to have promising mechanical properties.[2]

Materials and Methods: The synthesis of NW-templated 3DFG (NT-3DFG) involves a three step process: (i) synthesis of SiNWs through the catalyzation of gold nanoparticles on a Si substrate with a 600 nm wet thermal oxide via a vapor-liquid-solid (VLS) process; (ii) formation of a SiNWs mesh by collapsing the SiNWs using liquid nitrogen and annealing in hydrogen; and (iii) synthesis of 3DFG using plasma-enhanced chemical vapor deposition (PECVD) under the flow of methane with varying growth times. NT-3DFG was then characterized by scanning electron microscopy (SEM), ultraviolet-visible (UV-Vis) and Raman spectroscopy.

Results and Discussion: SEM characterization shows the out-of-plane growth of graphene flakes from the surface of the NWs.[2] It also reveals an increase in the size of the flakes with increase in growth times of 3DFG. UV-Vis characterization shows a significant increase in the absorbance post-3DFG synthesis (Figure 1). Absorbance values were 71, 82, 85, 94, and 96% for 0, 1, 5, 10, and 30 min NT-3DFG growth times respectively. Higher growth time led to higher absorbance due to an increase in the graphene flake size and density. The presence of D, G, and 2D peaks at ca. 1335, 1650, and 2700 cm^{-1} respectively in the Raman spectra confirmed the presence of graphene. The dual-wavelength Raman spectroscopy characterization revealed that the emergence of the D peak at ca. 1335 cm^{-1} is caused by breaks in translational symmetry due to the presence of 3DFG edges.

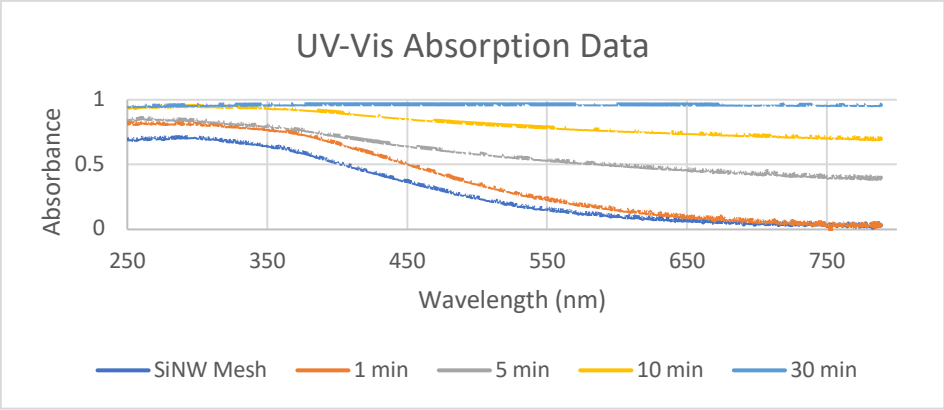

Figure 1. Absorbance spectra of SiNWs and NT-3DFG with varying growth times

Conclusions: Presence of 3DFG led to a significant increase in the absorption over a wide spectral window. The absorbance of NT-3DFG can be tailored by changing the 3DFG flake size and density. The high photo absorbance of NT-3DFG nanomaterial makes it a potential candidate to enable changes in local temperature at the nanomaterial-cell interface that can lead to stimulation of excitable cells with a high spatial precision. The future work will involve (i) a viability test of the NT-3DFG, (ii) photothermal current characterization of this nanomaterial to optimize the laser power and duration required to generate currents, and (iii) interfacing the nanomaterial with cardiomyocytes and photothermal stimulation. This platform will enable modulation of cellular networks with high precision and specificity which is crucial for evaluating arrhythmias and reducing artifact.

References:

1. Nicola Martino et al. *Scientific Reports*, 2015, 5, 8911.
2. Raghav Garg et al. *ACS Nano*, 2017, 11 (6), pp 6301-6311.

Experimental Model of Clot Formation in a Fiber Bundle Using 3D Printed Microscale Perfusion Chambers

Cameron Pitts

Introduction

The development of artificial lungs for destination therapy could provide a long-term solution to patients who suffer from lung disease and cannot receive a lung transplant. A great design challenge is faced in the development of artificial lungs: avoiding thrombus formation. When blood contacts an artificial surface, the intrinsic branch of the coagulation cascade is activated, which leads to thrombus formation that can cause device failure. Thrombus formation is particularly common in artificial lungs due to complex geometry and high surface area of the fiber bundle, the vital component for gas exchange. In order to determine how factors such as blood flow rate, path length, and bundle geometry affect coagulation, an experiment using 3D printed microscale perfusion chambers has been designed. This study explores a benchtop model for testing different artificial lung fiber bundle parameters and their effect on clot formation.

Materials and Methods

To 3D print the perfusion chambers, an Autodesk Ember printer was used. Each print was created with two different types of resin, clear and black. The thin layer of clear resin on the bottom of the device allows the microscope to illuminate the clots trapped within the device, while the black resin reduces the light from the resin autofluorescence Three different types of chambers where printed: 40%PD (packing density), 50%PD, and 60%PD. Each packing density represents the percentage of space that the rods in the design take up.

Once the chambers have been printed, whole, fresh human donor blood will be run through them at different anticoagulation concentrations. As the blood flows through the chamber, platelets will be activated and protein will adsorb to the surfaces, causing thrombus formation. Different time points will be used (5min, 10min, and 20min) to capture the clot at different points as it is forming. The clot will then be fixed in formaldehyde. Images of fibrinogen within the clots formed will be taken with a two-photon microscope (brand, location), and gross clot images will be taken with a light microscope (Nikon SMZ1000, Tokyo, Japan).

To create more clarity in identifying where clots had formed within the perfusion chambers, an algorithm was written in python that manipulates ambiguously colored pixels and changes them into one of three distinct colors: red, yellow, or black. When the algorithm was applied to the gross clot images, the boundaries separating the blood clots from the device were easily seen. ImageJ (National Institute of Health, Bethesda, MD) software was used to determine the RGB values of pixels that represented the device, the clot, and any other background color. The data provided by ImageJ showed trends in RGB pixel values that allowed the algorithm to be written.

Results and Discussion

The software Print Studio (San Rafael, CA) was used to manipulate the 3D printer settings for the printed perfusion chambers. Each of the three types of chambers required different print settings, as they were each slightly different chambers. Through iterations, the settings for the print supports, printer speed, number of burn layers, and more were refined. The settings and protocols for the 50% and 60% chambers have been solidified, while the 40% chamber is still being worked out.

In the future, the techniques used to image fibrinogen can be used to stain and image active and inactive platelets within clots. Indirect immunocytochemistry can be utilized in order to differentiate between the two platelet states within in a clot, and the two-photon microscope can be used to image the platelets.

The image analysis of the gross clot images allowed for comparison of clot formation in the perfusion chambers from this experiment to clot formation in the perfusion chambers of previous ones. This comparison allows for analysis of clot size and shape to be conducted based on the factors that we aimed to test.

Conclusion

The analysis of the gross clot images captured from this experiment, as well as the last, have allowed general observations of thrombus trends in the microscale chambers to be made. One of the key trends picked up on was that blood tends to clot by the outlet of the chambers as opposed to the inlet. Imaging of the fibrinogen stains is currently taking place, and the data from those images will provided further data regarding the characteristics of clot formation within the microscale device.

Acknowledgements

I would like to thank Angela Lai for all of her guidance and mentorship pertaining to this project. I would also like to thank the American Heart Association for providing the funding for my summer research via the Carnegie Heart Program.

Designing a Probe for Non-Invasive Measurements of Intercranial Blood Flow Using Diffuse Correlation Spectroscopy

Liliana Santizo
Kainerstorfer Lab, Department of Biomedical Engineering

Introduction

Normal intercranial blood flow is essential for proper tissue function, because it delivers nutrients and oxygen to tissue. If blood flow is abnormal, less nutrients are delivered to tissue. Abnormal intercranial blood flow is related to many health problems, such as head trauma and strokes [1]. If abnormal measurements of blood flow are found, proper treatments can be administered to return blood flow to normal. Current methods of intercranial measurements of blood flow are invasive and expensive. By using diffuse correlation spectroscopy (DCS), noninvasive measurements of intercranial blood flow can be made. The Kainerstorfer lab is developing a device that uses DCS to measure intercranial pressure and blood flow. A probe was developed over the summer to facilitate these measurements.

Methods and Materials

DCS is a scattering method that measures changes in light intensity, caused by movement of photons, over delay times [1]. With these measurements, the motion of red blood cells can be measured. To measure intensity changes, photons are sent through the head by a 785nm laser, and a detector, that is placed a few centimeters away from the light source, counts the photons that return. A pulse is generated for every photon that returns. With these pulses, fluctuations of light intensity can be determined. Then, when plugged into $g2(\tau) = \frac{I(t)I(t+\tau)}{(I(t))^2}$ [1], g_2 curves can be found. When plotted against delay times, g_2 curves help determine intercranial blood flow.

To design the probe that would hold the laser fiber and detector fiber, Solidworks was used. Then, the design was uploaded to a 3D printing software and sent to a 3D printer. Two types of printers were used when designing the probe. The first printer used, Ultimaker, had PLA as the print material and PVA as the support material. The 3D printing software used was Ultimaker Cura. The second printer used was a Formlabs printer, and it had gray resin as the print and support material. The 3D printing software used for the resin printer was Preform.

Results and Discussion

By creating several iterations of the probe, several parameters of the design were optimized. The optimal distance between the light source and the detector was determined to be 2.5cm, because at that distance, light can pass through the skull and into the brain. In order to prevent the fibers from being placed directly on the head, right angle prisms (PS905, Thorlabs) were used to redirect incoming light by ninety degrees into the head. The prisms were chosen to be 3mm long to make the probe as small as possible, thus ensuring the probe would fit on the forehead. It was determined that the optimal length of the probe was the length of the fiber tip. By making it this length, less light from the laser escaped, and the probe was still small enough to place on the forehead.

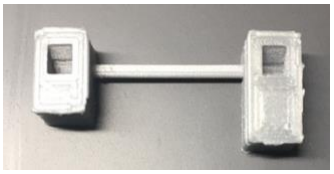

Figure 1. Probe with 2.5cm distance between fibers and cut out squares for the right angle prisms.

Conclusion

The probe is effective at maintaining a constant distance between the light source and detector fibers, and successfully redirects light by ninety degrees into the brain. By using the probe, collecting intercranial blood flow measurements is simpler, and DCS measurements are more accurate. Future studies should be performed to minimize light interference from the environment.

Acknowledgements

Thank you to Professor Kainerstorfer, Jason Yang and Alexander Ruesch for their guidance on the project during the summer.

References

1. Yu, Guoqiang, et al. *Near-Infrared Diffuse Correlation Spectroscopy for Assessment of Tissue Blood Flow.* www.physics.upenn.edu/yodhlab/papers/2011/Handbook_Biomedical_Optics_chpt10.pdf.

Realization of a Practical Robotic Device for Human Biomarker Research

Made possible by the CMU Summer Undergraduate Research Program (SURP). Investigator: Shanley Lenart.

Introduction: Molecular diagnostics, also called biomarkers, are becoming more popular in the medical field as powerful tools to achieve personalized medicine. Despite a large and growing number of known biomarkers, only about two new biomarkers are approved by the FDA each *decade*.

This project involved ongoing development of a microfluidic device for use by clinical researchers that can accelerate biomarker understanding by obtaining both patient data and biologic samples with minimal human intervention. Specifically, this SURP project focused on the optimization of this device by minimizing dead volume present within the device, and by increasing device hardiness. Luer lock intravenous connectors are widely used within the medical field where sterility is required, but are presently impractical for any microfluidic system because of excessive dead space. Therefore, this project first found a solution to minimize dead volume within these connectors, and secondly to create designs capable of withstanding disconnection forces. Thirdly, dead space in a microfluidic valve was also minimized. Finally, a physical connection between a fragile Peltier cooling chip, a heat sink and a double walled insulated sample collection container was optimized to protect the cooling chip while allowing easy sample removal.

Materials and Methods: Solidworks was utilized for the design of all 3D printed pieces. The Asiga 3D sterolithography printer was used for small parts, with a resin composed of Igracure 22 photo-initiator, polyethylene glycol diacrylate (PEGDA), and UV absorber 2,5-Bis(5-tert-butyl-benzoxazol-2yl)thiophene (TBT). The Ultimaker Original Fused Deposition 3D printer was also utilized with Polylactic Acid for the connector used on the insulated container. Luer locks were obtained from Grainger, and 0.5 mm cross-section and 1.5mm ID O-Rings were obtained from the O-Ring store. Furthermore, 150 um ID PTFE tubing, OD 1.58 mm from Western Analytical Tubing was used for the valve enclosure.

Results and Discussion: First, the Luer Lock male and female connectors were both modified to minimize the dead volume present using 3D printed glued inserts (Figs 1 and 2). Second, to solve the issue of accidental disconnection, a 3D piece was created as a support in between tube connectors. Viscous glue was injected into this piece, and provided stability for several connections throughout the device (Fig. 3). Third, a microfluidic valve was modified by shortening the tooth that divides two compressible silicone tubes (Fig. 4), preserving valve function but minimizing dead space added by the silicone tubes themselves. Finally, to create a connection incorporating the Peltier cooling chip, a 3D piece was created that had a collar that securely fastened to a copper heat pipe which conducts heat out of the sample container by attaching to the cold side of a Peltier chip. Support beams were also added to this piece, so that the 3D piece can integrate with expanding closed-cell foam insulation. The maintained R-7 insulation while allowing for easier sample removal without damaging the fragile thermoelectric cooling chip (Fig. 5).

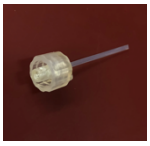

Figure 1: Glued inner microtubing inside male Luer Lock.

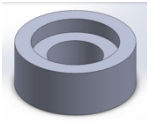

Figure 2: Female Luer Lock 3D printed insert markedly reduced dead space. A ridge was created to allow for the insertion of an O-Ring for a tight connection between the male and female Luer lock.

Figure 3: Design for 3D printed tube connector support with injection port

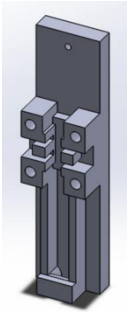

Figure 4: 3D printed valve enclosure.

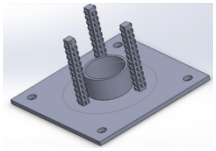

Figure 5: Connector for Peltier cooling chip and insulation container.

Conclusion: Ultimately, this project successfully optimized key components of the microfluidic device. By minimizing dead space the microfluidic samples transit to the cooler faster and are cooled more quickly, to preserve sample integrity. The use of familiar Luer Lock connectors fits in with decades of clinician practice preserving the sterility of intravenous lines. Robust connections minimize the chance of environmental contamination with potentially infectious biologic samples. The final device will be used in clinical research to further understand biomarkers within a clinical context. This device ultimately will accelerate precision medicine and assist in providing personalized treatments for patients in intensive care units and hospital wards.

The Use of Clinical Immersion to Develop Senior Design Projects

Shinjini Ray[1], Gabriela Pérez-Lozano[2]
Carnegie Mellon University Department of Biomedical Engineering
Department of Chemical Engineering[1], Department of Mechanical Engineering[2]

Introduction: This project utilized clinical immersion experiences to develop a list of projects for BME Senior Design. By entering clinical environments, the observers were able to see medical devices in use and identify areas for improvement. The observers spoke with therapists, surgeons, nurses, technicians, and other specialists about the issues they encountered in the workplace, as well as with patients and their families about challenges they encountered at home. These observations were recorded and researched to generate areas of study for BME Senior Design and the department.

Methods: The observers recorded all notes using paper and pen, including drawings of rooms and devices. This was in order to remain compliant with the Health Insurance Portability and Accountability Act (HIPAA). During a typical immersion experience, the individual being shadowed gave a brief explanation of the upcoming procedure or appointment. The observers were able to ask questions at appropriate times, and often requested more information about processes that seemed inefficient or difficult to complete. In settings where more than one professional was present, the observers were able to converse with them as well. In some appointments, the observers had limited patient contact, dictated by the individual being shadowed and the patients themselves. The observers were then able to ask about devices being used beyond a clinical setting. All of these observations were typed up and parsed through to compile a potential list of research projects. These projects were narrowed down with help from Dr. Zapanta, and the final selections were written up with background research and context.

Results and Discussion: The clinical immersions were scheduled with five departments at two institutions: Allegheny General Hospital and The Children's Institute. At Allegheny General Hospital, the procedures observed were with the Departments of Thoracic and Orthopedic Surgery. At The Children's Institute, the observers sat in on outpatient appointments with Physical, Occupational, and Speech and Language Therapy. In total, approximately 45 hours of observation were completed. The notes from these observations were digitized and used to create a list of 31 potential projects. Of these, 12 were selected for more research. These decisions were made based on the parameters of the course and the skill level of the students taking it. For example, one potential project is the development of a gait trainer that reinforces reciprocal gait. Another potential project is creating a more efficient heat exchanger for use with a cardiopulmonary bypass machine. The study also generated ideas that were beyond the scope of the course but could be interesting for other departments to pursue. This includes a HIPAA-compliant communication app for healthcare professionals and an online database of demonstrational videos for patients in occupational therapy.

Conclusion: Clinical immersion allowed for a real-world perspective that would otherwise be unavailable to students. This perspective led to several important observations. Any project is only viable if it is cost-effective or can be covered by insurance, and it can be vulnerable to transitional issues once it is replaced. Web-based applications are a new area of exploration for therapies, and they are continually being improved. As such, future work could rely on the involvement of Computer Science majors with the design projects. Another area for improvement is the expansion of the summer research program. If more departments are available for shadowing, representatives from each engineering discipline would be able to contribute to the list of project ideas. This would ensure a more even spread of project opportunities across departments.

Acknowledgements: Dr. Conrad M. Zapanta *Carnegie Mellon University Department of Biomedical Engineering*
The Children's Institute:
Amy O'Donnell, Lisa Kennedy, Christy Neltner, Kit Concilus, Maria Tozzi, and Chris P *in Physical Therapy*
Mary Jo Smith, Kaitlin Goerl, Lynn Winters, Blythe Westendorf, and Catherine Leece *in Occupational Therapy*
Colleen Chester, Jackie McCluskey, Katie Hartman, and Kathy Garrett *in Speech and Language Therapy*
Allegheny General Hospital:
Dr. M. Scott Halbreiner *in the Department of Thoracic Surgery*
Dr. Greg Altman, Dr. Trish Melvin, and Traci Salopek *in the Department of Orthopedic Surgery*

Synthesis and characterization of tPA conjugated microbubbles for possible future application as a theranostic agent in treatment and prognosis of sonothrombolysis or sonoreperfusion

Courtney Ollis

Introduction: Tissue plasminogen activator (tPA) is a serine protease found on endothelial cells, which enzymatically catalyzes the conversion of plasminogen to plasmin- the major enzyme involved in the breakdown of blood clots (**Figure 1**). Due to this thrombolytic activity, the recombinant version of tPA (rtPA) has been approved by US Food and Drug Administration (FDA) for medical treatment of microvascular obstruction (MVO) based cardiac disorders such as acute myocardial infarction (AMI), acute ischemic stroke (AIS) and acute massive pulmonary embolism. While exogenous administration of rtPA to eligible patients has been proven to improve functional outcomes, however, bleeding complications due to excessive thrombolytic activity may lead to adverse side effects in the form of an intra-cerebral hemorrhage[1]. Therefore, it is not only necessary to reduce the pharmacologic dose of rtPA without reducing required therapeutic activity, but also necessary to closely monitor the microvascular system during the treatment with appropriate clinical imaging modality. One such cardiovascular imaging modality approved by the FDA involves ultrasound (US) contrast agent comprising microbubbles (DEFINITY®) filled with octafluoropropane gas. In addition, several MVO based preclinical studies involving similar microbubbles (MB) have reported enhanced reperfusion in the microvasculature due to ultrasound-induced MB oscillations imparting shear stress on the surrounding medium[2]. Therefore, we hypothesize that by conjugating rtPA onto these MBs, it is possible to reduce the required dose of tPA without reduction in therapeutic activity due to synergistic effects from tPA, US and MBs, as well as simultaneously monitoring microvasculature for disease prognosis. In this study, we intend to synthesize a theranostic molecule in the form of tPA conjugated MBs (tPA-MBs) and ascertain their therapeutic activity by a tPA functional assay.

Materials and Methods: Phospholipid-encapsulated MBs containing perfluorocarbon gas were synthesized according to the previously reported protocol[3] with appropriate modifications, where, 1,2-distearoyl-sn-glycero-3-phosphocholine (DSPE)-peg-biotin (Laysan Bio Inc.) was used instead of DSPE alone. The resulting microbubbles with biotin molecules were conjugated with rtPA (Alteplase, Genentech) via streptavidin (Sigma) crosslinking and NHS conjugation chemistry using NHS-PEG4-biotin (Thermo Scientific). The concentration and diameter of tPA-MBs was determined by a Multisizer (Beckman Coulter). The success of the tPA conjugation and quantity of tPA loading in each step was ascertained by using a Bradford protein Assay (Bio-Rad). The unconjugated tPA and Streptavidin were removed via centrifugation in 30 KD and 100 KD protein filters (Thermo Scientific). The functional activity of tPA-MBs was determined by chromogenic plasmin substrate (D-Val-Leu-Lys-p-Nitroanilide Dichloride, Sigma).

Results and Discussion: The concentration of the MBs (**Figure 2 &3**) before and after conjugation with tPA were found to be 1.234×10^9/mL and 0.883×10^9/mL respectively. Similarly, average diameter of the MBs (**Figures 2 &3**) before and after conjugation with tPA was found to be 2.859 μm and 3.533 μm respectively. The tPA conjugation procedure involves centrifugation of MBs to remove unbound tPA-Biotin-Streptavidin, which leads to simultaneous removal of smaller sized MBs. This explains the decrease in concentration and increase in average diameter of tPA MBs. The amount of protein in tPA-Biotin, tPA-Biotin-Streptavidin and tPA-MBs as determined from the Bradford standard curve (**Figure 4**) was ~563μg/mL, ~1.342 μg/mL and ~0.611μg/mL respectively. The amount of tPA in tPA-Biotin-Streptavidin and tPA-MBs was estimated to be ~268-223 μg/mL and ~ 122-102 μg/mL respectively. Although efficiency of tPA loading was quite low (10-12%) compared to initial tPA, the functional assay (**Figure 5**) showed significant increase in tPA activity compared to control MBs. This confirms the tPA conjugation with MBs as determined by quantitative Bradford assay. Additionally, tPA conjugated biotin showed similar functional activity compared to tPA alone at the same concentration. This result is significant in the sense that biotin conjugation does not seem to interfere in tPA functional activity of converting plasminogen to plasmin.

Conclusions: The successful conjugation of tPA on to the MBs without reduction of functional activity was confirmed both by the quantitative Bradford assay and the tPA functional activity assay. The tPA loading efficiency can be improved with appropriate optimization of the current protocols. Additional *in vitro* and *in vivo* preclinical research will allow confirmation of sonothrombolysis/sonoreperfusion activity of tPA-MBs with simultaneous monitoring of microvasculature via US imaging. The above results indicate the future application of tPA-MBs as theranostic agent for the treatment and prognosis of MVO based cardiovascular disorders.

References

1. Gravanis, I.; Tsirka, S. E., Tissue-type plasminogen activator as a therapeutic target in stroke. *Expert Opinion on Therapeutic Targets* **2008,** *12* (2), 159-170.
2. Goyal, A.; Yu, F. T. H.; Tenwalde, M. G.; Chen, X.; Althouse, A.; Villanueva, F. S.; Pacella, J. J., Inertial Cavitation Ultrasound with Microbubbles Improves Reperfusion Efficacy When Combined with Tissue Plasminogen Activator in an In Vitro Model of Microvascular Obstruction. *Ultrasound in Medicine & Biology* **2017,** *43* (7), 1391-1400.
3. Yu, F. T. H.; Chen, X.; Straub, A. C.; Pacella, J. J., The Role of Nitric Oxide during Sonoreperfusion of Microvascular Obstruction. *Theranostics* **2017,** *7* (14), 3527-3538.

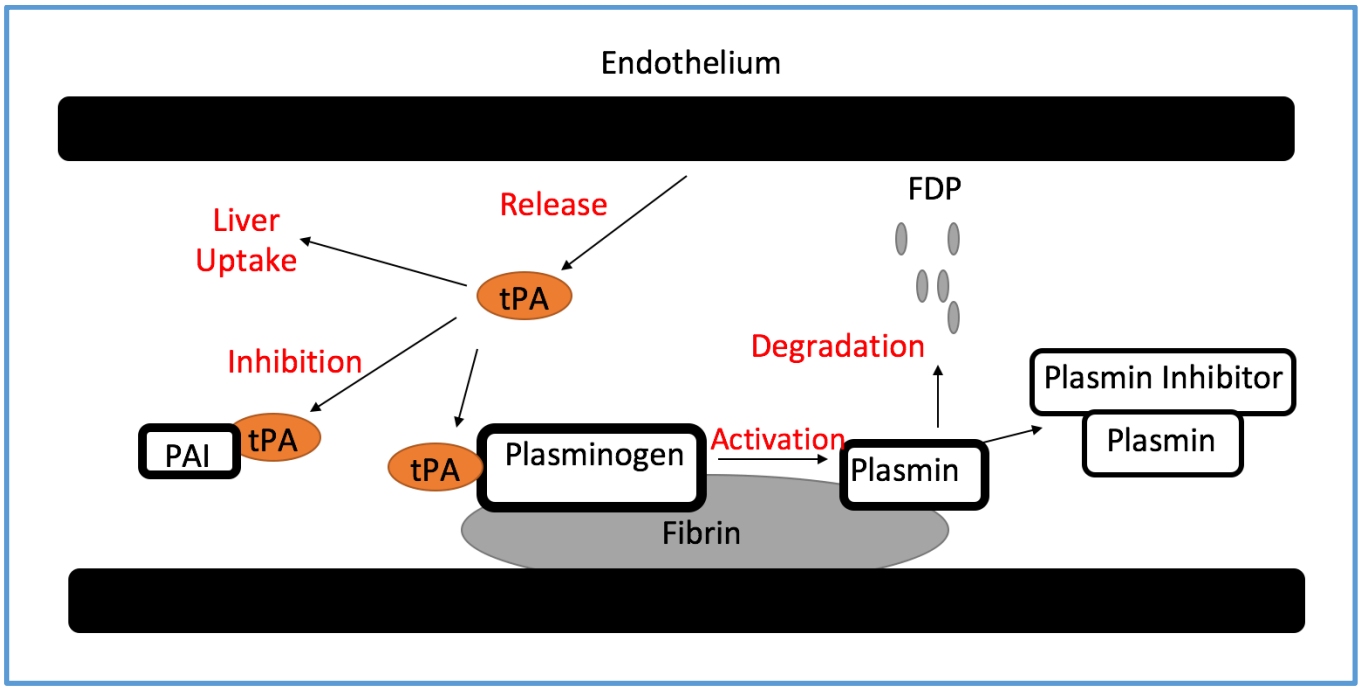

Figure 1: In vivo mechanism of action of tPA within the fibrinolytic system. tPA can go one of three ways in the body; (1) uptaken by the liver and cleared through receptors therein, (2) inhibited by a plasminogen activator inhibitor (PAI) and subsequently cleared from the liver, or (3) through the activation of plasminogen to plasmin for degradation to result in fibrin degradation product (FDP). (*diapharma.com*. Retrieved 07-23-2018)

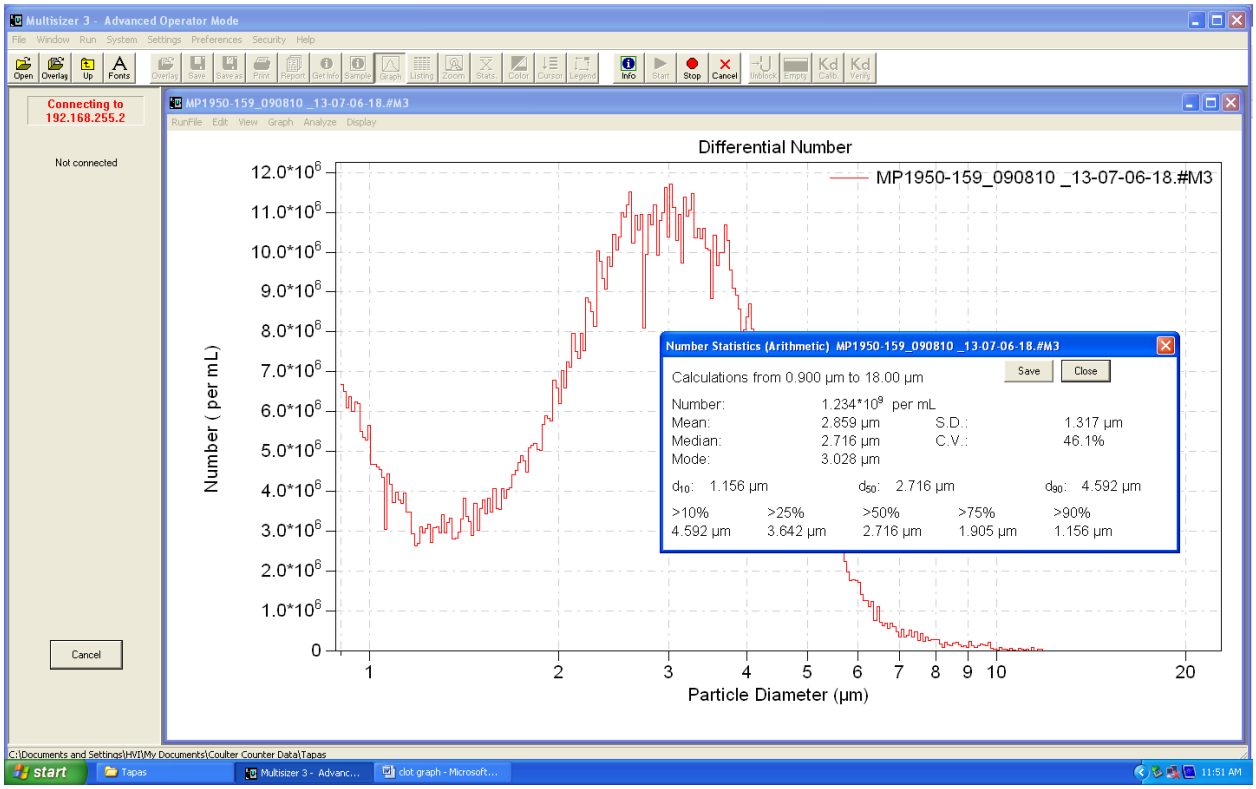

Figure 2: Concentration and average diameter of MBs before tPA conjugation as determined by Multisizer.

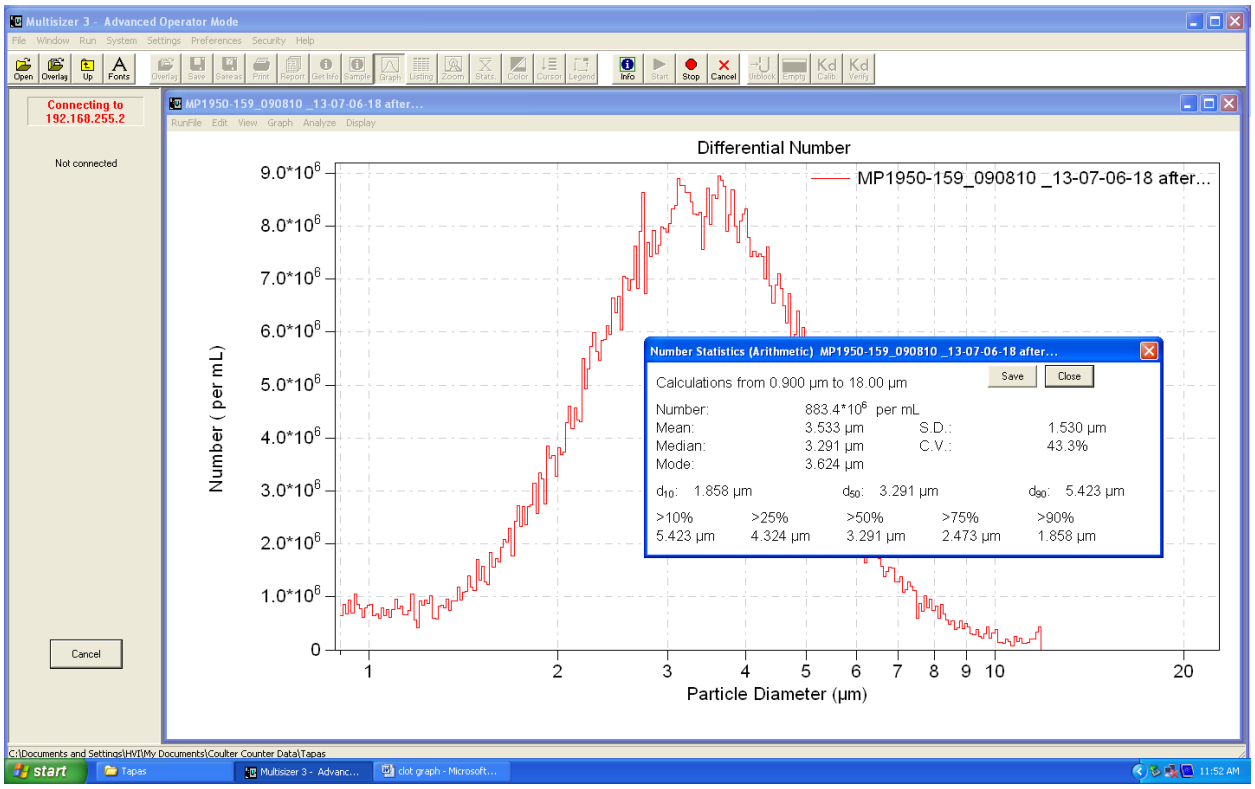

Figure 3: Concentration and average diameter of MBs after tPA conjugation as determined by Multisizer.

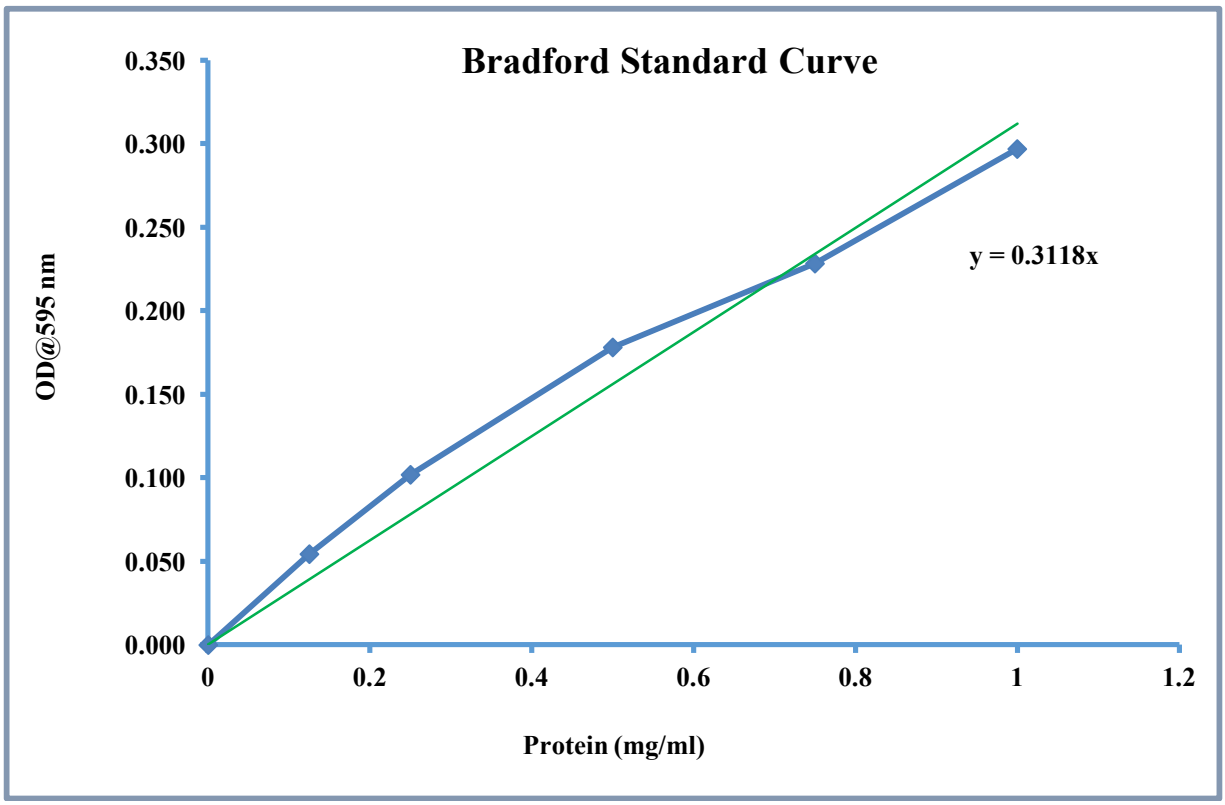

Figure 4: Protein standard curve prepared using quantitative Bradford assay of known quantity of Bovine serum albumin (BSA).

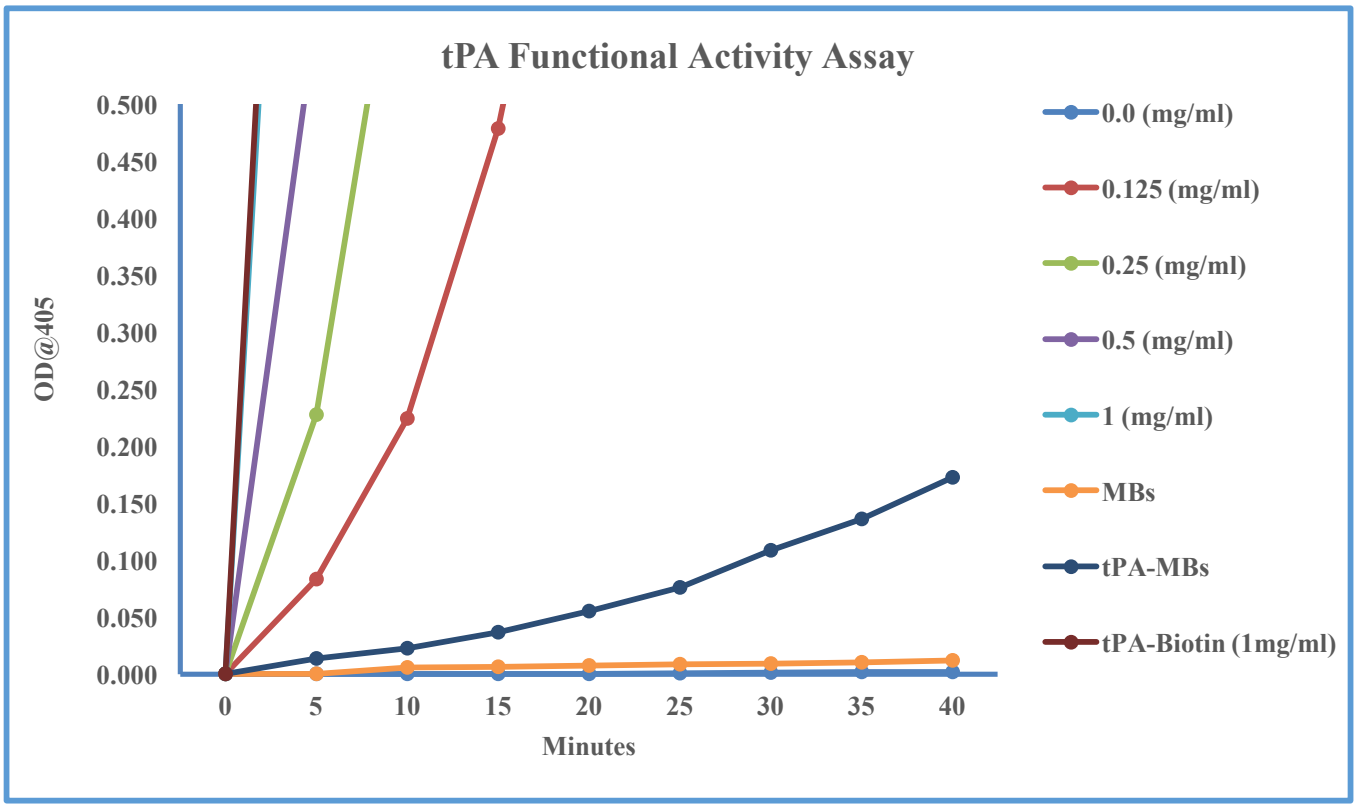

Figure 5: tPA functional Activity Assay showing catalytic conversion of plasminogen (100µg) in to plasmin, which in turn converts its chromogenic substrate

Andrew Febrillet

Introduction:

Artificial organs provide patients with a life saving alternative to organ transplantation. Rather than losing precious time waiting for an appropriate donor, patients may opt for an artificial organ transplant instead as a more readily available option. However, current biomaterials used to make these artificial organs fall short in areas of selectivity and design. A material with adequate permeability and resistance to functional degradation caused by protein adsorption is needed. The focus of this project is to develop non-fouling, semipermeable hydrogels as fundamental materials for organ engineering to resolve this underlying issue in artificial organ development.

Materials and Methods:

A solution consisting of 30% Acrylamide/Bis solution 29:1 (3.3% crosslinker) and Double distilled water in a 1:3 ratio (acrylamide:water) was created and polymerized to form a non-porous hydrogel. Hydrogels are more likely to resist adsorption because of their hydrophilic nature; water essentially forms a shield-like layer on the gel that keeps proteins from contacting the material and adsorbing to it. The interaction between water and the polymer hydrates the surface, expanding the hydrophilic polymer chains along it and thus furthering this shield-like effect. Tetramethylethylenediamine (TEMED) and a 1.5 mg/ml solution of Lithium Phenyl 2,4,6-trimethylbenzoyl phosphate (LAP) were used as polymerization catalyst and agent, respectively.

Urea salt crystals ratio were added in a 1:1 (solute:solvent) to and dissolved in the hydrogel solution (above) before polymerization. The ratio of acrylamide:water was adjusted to 1:1 with the inclusion of urea in the solution. The solution vessel was submerged in ice then agitated on a mixer to induce crystallization then returned to heat to dissolve. This process was repeated multiple times to create crystals of varying size. After polymerization, the crystals were dissolved away leaving behind a network of channels; the crystals served the purpose of providing the material with increased permeability.

To determine the effect of channel size on rate of flow through the gel, a 1.5 mg/ml sample of Tetramethylrhodamine isothiocyanate-Dextran (155 kDa) was allowed to diffuse through the gel into an outside solution of Phosphate buffered saline (PBS). Samples were drawn periodically from this solution and their fluorescence measured. The fluorescence readings over time were plotted and their slopes, corresponding to relative rates, compared between gels of varying channel size.

Results and Discussion:

Methodology (temperature control, crystallization cycling, agitation, etc.) to create gels with specific channel sizes was standardized. To create gels with small channels, solution vessel must be submerged in ice for 3 minutes before agitation for the first cycle. Succeeding cycles (at least 2 for small crystals) must be kept on ice for only 1.5 minutes before agitation. After reaching desired number of cycles, the solution must be transferred to a separate vessel to conform to the vessel's shape and be kept on ice another 2 minutes to allow for further crystallization before polymerizing, while still on ice, for 7-9 minutes. This process was found to be effective for creating gels with moderately sized channels as well except the amount of cycling must be restricted to a single cycle. For large channels, it must also be restricted to the single cycle but be kept submerged for 3.5 minutes instead of 3 minutes.

Previously obtained data for determining relative flow rates (i.e. **Figure 1**) has been found to be unreliable due to undetected leaks. Rates lacked consistency and were substantially higher than recently obtained data, which is still being conducted and standardized.

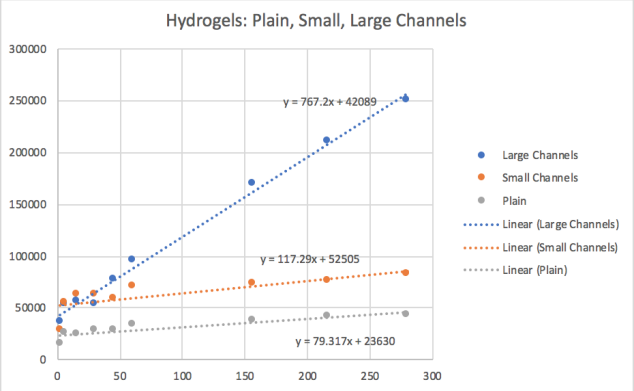

Figure 1. As expected, the larger channels allow a substantially higher rate through than the smaller ones and the plain gel, without any engineered channels.

Conclusion:

From data gathered on rates thus far, a hydrogel with larger channels may be preferred as smaller channels allow minimal flow through them if unassisted by an outside force. Larger channels allow a greater degree of flow through so a greater amount of media can reach underlying cells thus maximizing cell survivability.

Looking ahead, fluorescent beading is to be used to determine relative channel size in each gel. This is to be conducted in a similar fashion to the procedure involving Dextran (above).

Lastly, a survival test is to be conducted; plating the gels with cells and media to determine degree of bioavailability and confirm whether large channels are ideal for the biomaterial.

Acknowledgements:

The author would like to acknowledge and thank Professor Yu-Li Wang for the opportunity to undertake this project and his guidance throughout it. The author would also like to thank the Summer Undergraduate Research Experience (SURE) program for providing the funding that has allowed him to continue the project this summer.

References:

The Effect of Genipin-induced Crosslinks and Genipin Dose on Clot Stability

Xuanyu(Leon)Min

Introduction: In the U.S, more than 30,000 individuals suffer brain aneurysm each year. Of those afflicted, there is a 30%-40% mortality rate for patients with a ruptured aneurysm due to intracranial hemorrhage. Currently, one surgical procedure to treat aneurysm is endovascular coiling. A platinum coil is released It induces clotting of the aneurysm or the formation of fibrin, as the coils are registered as foreign object. Ideally it prevents ruptures by blocking blood flow into the aneurysms. However, there is still a possibility for aneurysm rupture even after the procedure due to the instability of the clot. The fact that aneurysm recurrence after coiling occurs in 34% of patients should not be ignored. Our research has found that genipin, an extract from gardenia flower, forms crosslinks with amines in fibrin. The relationship between genipin to fibrin concentration ratio and its effect on stability of the clot has been studied.

Materials and Methods: In order to study genipin dose and its effect on clot stability, samples with 0(fibrin only), 1:1, 1:10 genipin to fibrin concentration ratio were made. Clots were made by mixing thrombin and fibrinogen from bovine plasma and different doses of genipin were added into the clots at the same time. Samples were then incubated for 24 hours at 37 degree Celsius to allow crosslinks to form. After gelation, rheology test was conducted on each sample. Frequency sweep measured the storage modulus, which reflects the stiffness of the samples.

Results and Discussion: Based on the rheology result, it showed that the genipin-induced crosslinks in fibrin increased the storage modulus or the stiffness of the clots. Moreover, the higher the concentration of genipin, the higher the stiffness of the clots, as 1:1 genipin to fibrin concentration ratio yielded a larger storage modulus than the 1:10 ratio. The increase of the stiffness of the clots due to genipin-induced crosslinks has a significant impact on clots stability, as it mechanically stabilizes the clots by reducing compaction from blood pressure, therefore, preventing the rupture of brain aneurysms.

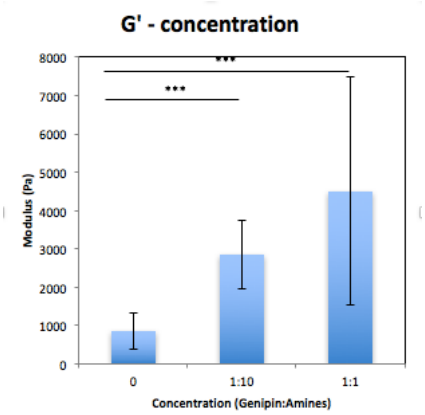

Figure 1. The effect of genipin-induced corsslinks and genipin dose on stiffness of fibrin.

Conclusions: Genipin-induced crosslinks increase the stiffness of clots, therefore mechanically stabilizing the clots by reducing the compaction from blood pressure and potentially preventing the rupture of brain aneurysms. In the future, the effect of dosing time of genipin on clot stability should be studied.

Acknowledge: I would like to thank Prof. Christopher Bettinger, who gives me instruction on the project and Chen Chen, who assisted in conducting rheology test.